Synthesis and Optical Properties of CdS Nanoribbons

Soumitra Kar,[†] B. Satpati,[‡] P. V. Satyam,[‡] and S. Chaudhuri*[,†]

Department of Materials Science, Indian Association for the Cultivation of Science, Kolkata 700 032, India, and Institute of Physics, Bhubaneswar 751 005, India

Received: May 17, 2005; In Final Form: July 22, 2005

Rapid production of single crystalline CdS nanoribbons with hexagonal wurtzite phase has been achieved by thermal evaporation of CdS powder on Si wafers. The flow rate of the carrier (Ar) gas along with the synthesis temperature plays an important role in defining the size and shape of the CdS nanoribbons. Scanning electron and transmission electron microscopic observations revealed the nanoribbons to have a flat end as well as side surfaces which will make it ideal for optoelectronic devices such as nanolasers and light emitting diodes based on individual nanoribbons. The nanoribbons have widths within 200−400 nm and lengths approximately a few hundred micrometers. Room-temperature photoluminescence measurements show green emission centered at ∼525 nm which may be ascribed to the near band edge emission. The Raman spectra of the CdS nanoribbons show peaks around 304, 609, 915, and 1220 cm^{-1} corresponding to the first-, second-, third-, and fourth-order longitudinal optical phonon modes, respectively.

1. Introduction

Since the first discovery of carbon nanotubes, one-dimensional (1-D) semiconductor materials have attracted extensive interest because of their fundamental importance and wide range of potential applications in nanoscale devices.[1−9] Semiconductor nanoribbons/nanobelts have been reported as a new subgroup of 1-D nanostructures[10] which are distinctly different from nanotubes and solid nanowires. Over the past few years a variety of oxide (ZnO,[10−11] SnO_2,[12] Ga_2O_3,[13] and In_2O_3,[14] etc.), nitride (GaN [15]), and sulfide (ZnS [16,17] and CdS[18−21]) nanobelts/nanoribbons with a rectangular cross-section and perfect crystallinity have been reported. Among them, CdS is an important II−VI semiconducting material used for a host of applications in optoelectronics such as nonlinear optics, flat panel displays, light emitting diodes, lasers, and thin film transistors, etc.[19−25] Recently, a thin film transistor has been fabricated on CdS nanoribbons,[19] and lasing was observed on individual CdS nanoribbons. For these kinds of applications, the end as well as side surfaces should be flat so that they may act as reflecting mirrors. CdS nanoribbons have been reported earlier by different routes.[18−20] Dong et al.[18] have reported the production of CdS nanoribbons and nanowires on tungsten substrate. Duan et al.[19] have synthesized CdS nanoribbons by vapor transport method. Liu et al.[20] have produced CdS nanoribbons by Au-mediated vapor−liquid−solid (VLS) method. All these methods were time-consuming, as these processes required 2−2.5 h for the fabrication of CdS nanoribbons. Also from earlier reports it was noticed that the temperature of the source and the position of the substrate can influence the morphology and size of the products fabricated by thermal evaporations routes such as VLS or vapor−solid (VS) mechanism. But the impact of the flow rate of the Ar gas (used as the carrier gas of the source vapor) on the size and shape of the nanoforms remains unexplored. In fact the flow rate of the Ar gas is an important physical parameter in the above-mentioned synthesis techniques and needs attention to get morphological control over the synthesized nanoforms.

Here, in this paper, we report the Au-mediated rapid growth (30 min deposition time) of CdS nanoribbons on Si substrate. The role of the flow rate of the Ar gas and the temperature on the size and shape of the CdS nanoribbons are studied. Moreover, the luminescence and Raman properties of the as-synthesized products are also investigated.

2. Experimental Section

Details of the experimental setup for the preparation of CdS nanoribbons have been described elsewhere.[17] In short; a conventional horizontal tube furnace was used for the synthesis. Si (100) wafers used, as the substrates, were first ultrasonically cleaned in acetone for 20 min and then sputter-coated with a thin (∼25 Å) layer of Au film. CdS powder, used as the precursor, was prepared through a chemical route by adding aqueous Na_2S solution dropwise to the aqueous solution of $Cd(NO_3)_2 \cdot 4H_2O$ with vigorous stirring, and Ar gas was bubbled through the aqueous solution of $Cd(NO_3)_2 \cdot 4H_2O$ to prevent oxidation. The yellow precipitate thus obtained and was washed successively in deionized water and absolute ethanol, and it was then dried in a vacuum at room temperature. A 0.5 g amount of the above-mentioned powder was loaded into a quartz boat. The Si substrate was then clipped over the boat with Au-coated surface facing the CdS powder in such a way that the vertical distance between the CdS powder and the Si substrate was ∼3 mm. The quartz boat was then placed near the closed end of a quartz tube. After evacuating the quartz tube to a pressure of 10^{-3} Torr, Ar gas was flown through it and was maintained for the entire deposition period. This precaution was required to eliminate O_2 and avoid any sort of oxidization. The quartz tube was then inserted into the preheated tube furnace, and after 30 min of deposition, it was taken out of the furnace to allow rapid cooling to room temperature. The deposition temperature was maintained at 900 and 950 °C for two sets of deposition, and

* Corresponding author. Tel.: +91-033-2473-4971. Fax: +91-033-2473-2805. E-mail: mssc2@iacs.res.in (S.C.); kar_mitra@yahoo.co.in (S.K.).
[†] Indian Association for the Cultivation of Science.
[‡] Institute of Physics.

10.1021/jp052600w CCC: $30.25 © 2005 American Chemical Society
Published on Web 09/28/2005

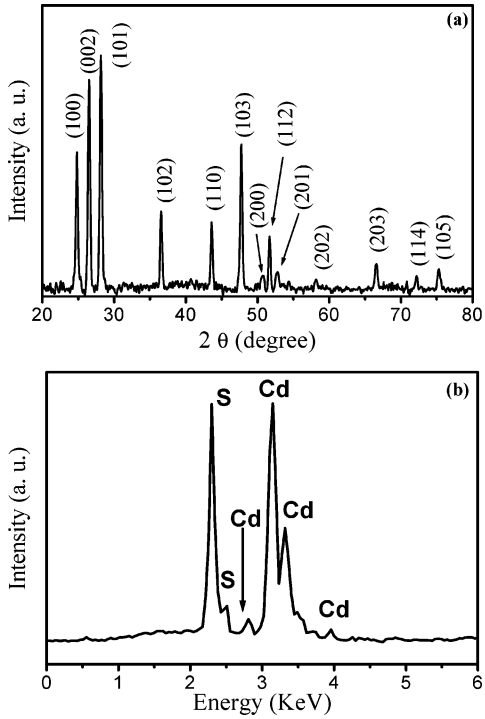

Figure 1. (a) XRD pattern of one of the representative CdS nanoribbons and (b) EDAX spectra recorded over a bunch of nanoribbons.

the flow rates of the Ar gas were fixed at either 200 or 800 cm^3(STP)/min for each set of temperatures.

The products were characterized by X-ray diffractometer (XRD, Seifert 3000P) with Cu Kα radiation, and the compositional analysis was done by energy dispersive analysis of X-ray (EDAX, Kevex, Delta Class I). Microstructures of the nanoforms were studied by scanning electron microscopy (SEM, Hitachi S-3200) and transmission electron microscopy (TEM, JEOL 2010). The high-resolution transmission electron microscopic (HRTEM) images and the typical selected area electron diffraction (SAED) patterns of the CdS nanoribbons were also recorded. Photoluminescence (PL) measurements were carried out at room temperature with a luminescence spectrometer (Perkin-Elmer, LS50B) using 400 nm as the excitation wavelength. Raman spectra were recorded using a SPEX 1403 monochromator equipped with a dc detection device. The 488 nm laser line of an Ar ion laser was used for excitation with an output power of 20 mW.

3. Results and Discussion

3.1. Structural and Compositional Studies. The yellow layers, deposited on the Au-coated surface of the Si wafer, were identified as CdS by the XRD. Figure 1a shows the XRD spectrum of a representative product having all the peaks corresponding to the hexagonal wurtzite phase of CdS with lattice constants $a = 4.14$ Å and $c = 6.72$ Å. These match well with those in the JCPDS card (Joint Committee on Powder Diffraction Standards, card no. 41-1049). The chemical composition and the stoichiometry of the CdS nanostructures were investigated through EDAX. Figure 1b shows the EDAX spectra recorded on a bunch of nanoribbons, revealing the chemical purity of the nanoribbons. Elemental analysis reveals the atomic percentages of Cd and S to be 51.2 and 48.8, respectively, which is consistent with the stoichiometric CdS within experimental error.

3.2. Microstructural Studies. For the microstructural analyses, the products were directly transferred to the SEM chamber

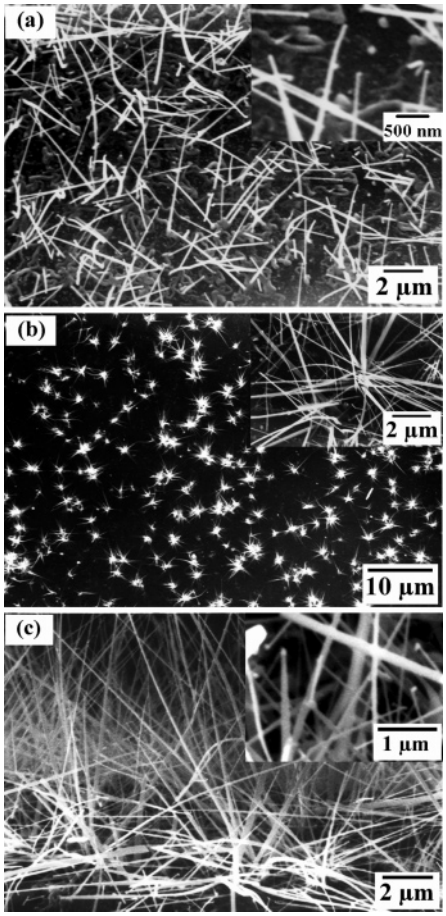

Figure 2. SEM image of the CdS nanoribbons synthesized at 900 °C with different Ar flow rates: (a) 200 and (b, c) 800 cm^3/min. Images a and b represent the CdS nanoribbons formed on the surface of the Si wafer, whereas c shows the CdS nanoribbons produced at the downstream edge of the substrate. Insets in all three figures show the closure view of these nanoribbons.

without affecting their original nature. It was observed that the morphology and size of the CdS nanoribbons depend on the synthesis temperature as well as the flow rate of Ar gas. Figure 2 shows the SEM image of the product obtained at 900 °C. When the flow rate of Ar gas was 200 cm^3/min, swordlike nanoribbons were found lying all over the Si substrate. The inset shows a closer view of these CdS nanoribbons, revealing the presence of Au nanoparticles at their tips. The composition of the nanoparticles present at the tips of the nanoribbons was also studied through EDAX, and unlike the results obtained from the body of the nanoribbons where only Cd and S were detected, the presence of Au along with Cd and S was confirmed at the particle area. Lengths of the CdS nanoribbons were ∼5 μm, whereas widths of these nanoribbons at their base were ∼200 nm, which decreased gradually toward their tips. The diameters of the Au nanoparticles were ∼50 nm. Instead of the uniform distribution of the nanoribbons (as mentioned above), randomly distributed starlike assemblies of CdS nanoribbons were observed with an increased Ar flow rate (800 cm^3/min) when all other experimental conditions were kept unchanged (Figure 2b). The magnified SEM image shown in the inset of Figure 2b revealed that these starlike assemblies were composed of several swordlike CdS nanoribbons. The sizes and shapes of these CdS nanoribbons were similar to those obtained in the previous case. At the same experimental condition, longer nanoribbons (length ∼ 10 μm) were also observed in large population at the downstream edge of the Si substrate (Figure 2c). A closure view

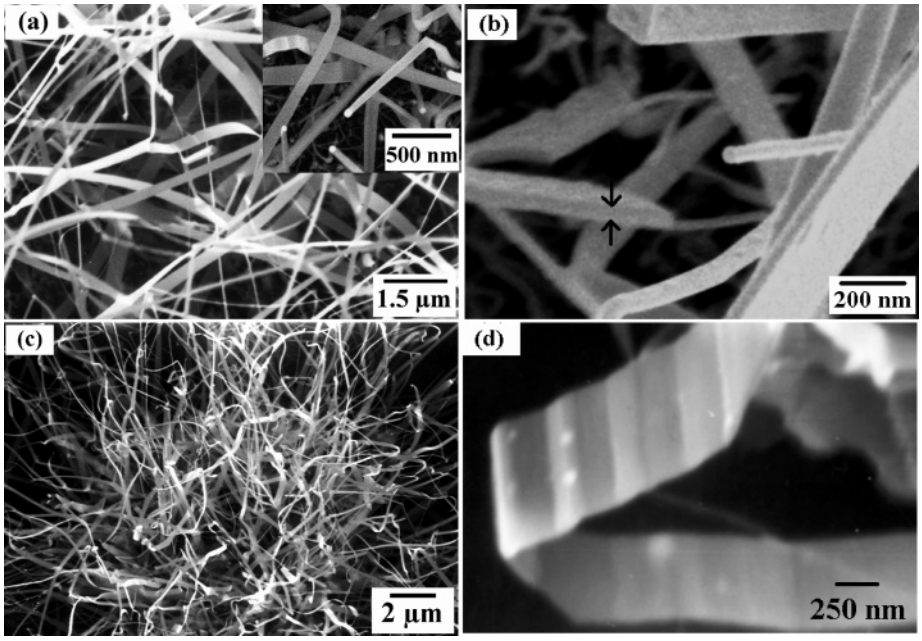

Figure 3. SEM image of the CdS nanoribbons synthesized at 950 °C with different Ar flow rates: (a and b) 200 and (c and d) 800 cm^3/min. The image shown in the inset of a reveals the presence of Au particles at the tips of the CdS nanoribbons. The arrow in the magnified image shown in b indicates the thickness of a CdS nanoribbon. The image in d reveals the wavy nature of the ribbons produced at higher Ar flow rate.

of these CdS nanoribbons also indicates the presence of Au nanoparticles at their tips (inset of Figure 2c). Figure 3a shows the SEM image of the nanoribbons obtained at 950 °C with an Ar flow rate of 200 cm^3/min. The nanoribbons obtained in this condition were a few hundred micrometers in length, and their widths varied within 200−300 nm. The widths of these nanoribbons were uniform throughout their length, except at the growth front, where they were again swordlike. Au nanoparticles were also observed at the tips of these nanoribbons as revealed by the SEM image shown in the inset of Figure 3a. Figure 3b shows the magnified SEM image of the CdS nanoribbons from which the thicknesses of the CdS nanoribbons could be estimated. Thicknesses of the CdS nanoribbons were ∼50 nm, which was of the order of the diameter of the Au nanoparticles. In fact, the thicknesses of the CdS nanoribbons could be controlled by controlling the sizes of the Au nanodroplets. Starlike CdS nanoribbon assemblies were also observed at 950 °C (Figure 3c) when the flow rate of Ar gas was increased to 800 cm^3/min. These nanoribbons were not straight and smooth throughout their length but wavy toward their growing end, which was evident from the magnified SEM image of a single CdS nanoribbon (Figure 3d). Figure 4a shows the bright-field TEM image of the CdS nanoribbon. The ripples like contrasts observed in the nanoribbon were due to the strain caused by the bending of the nanoribbon. The crystal structure of the CdS nanoribbons was further studied from their HRTEM images and SAED patterns. One representative HRTEM image of a single CdS nanoribbon is shown in Figure 4b, and the corresponding SAED pattern is shown in the inset. Both patterns revealed that these CdS nanoribbons were perfectly single crystalline, having hexagonal wurtzite structure. The measured spacing of the lattice fringes in the HRTEM image was 3.36 Å, which corresponds to the (002) plane of the wurtzite CdS. This (002) direction was also the growth direction of the CdS nanoribbons, and this was also confirmed from the SAED pattern. The (100) lattice plane corresponding to the hexagonal wurtzite CdS is also indicated in the SAED pattern.

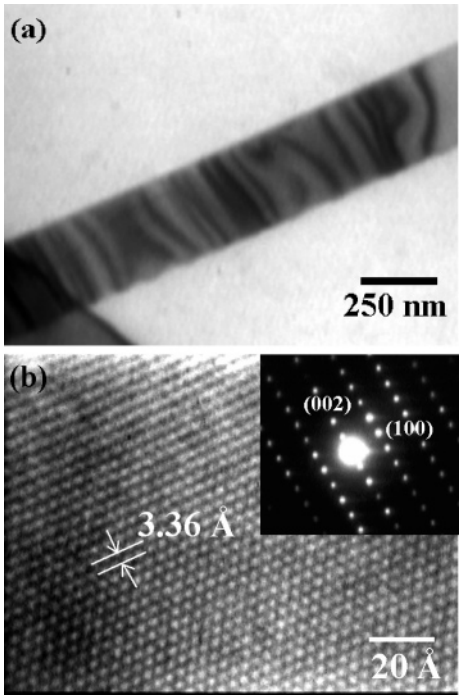

Figure 4. (a) TEM image of a CdS nanoribbon and (b) HRTEM image of the CdS nanoribbon along with the corresponding SAED pattern in the inset.

3.3. Growth Mechanism. Two well-established routes for the growth of nanoribbons/nanobelts are VS[10,16,21] and catalytic assisted VLS[17,18] methods. In the VS method the source materials vaporize to the molecular level with stoichiometric cation−anion molecules, which condensed to the substrate, and the molecule will be arranged in such a way that the proper local charge balance and the structural symmetry are maintained, resulting in a nucleation center. With further intake of the molecules, the surfaces that have lower energy, e.g. side surfaces, start to form and the low-energy surfaces tend to be flat. As the molecules have higher mobility at the high growth temperature, the newly arrived molecules tend to diffuse to the

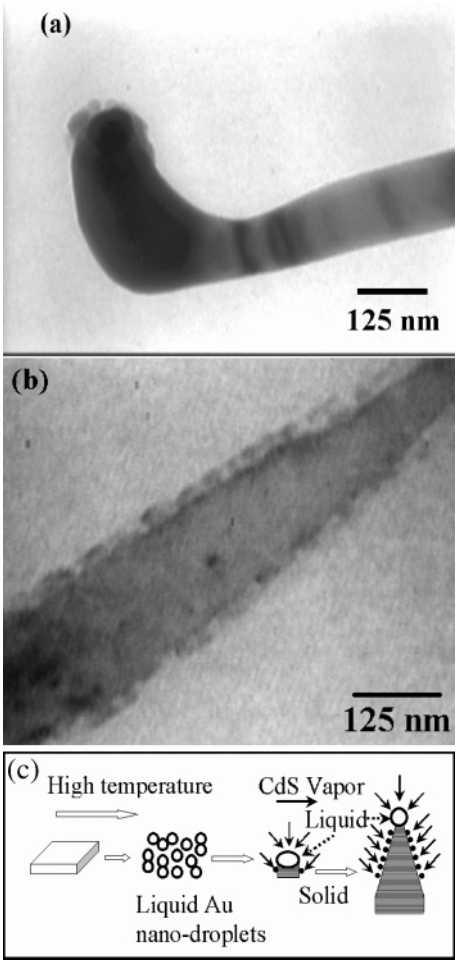

Figure 5. TEM images of the CdS nanoribbon: (a) tip containing the Au nanoparticles and (b) the rough growth front indicating the role of the VS mechanism. (c) Schematic view of the growth model.

rough growth front, resulting in the increase in the surface area, which leads to the formation of the nanoribbons. The rough surface at the growth front leads to the rapid intake of the incoming molecules, resulting in the rapid formation of nanoribbons. The newly arrived molecules can stick to the rough growth front or the side surfaces. But the smooth side surfaces and the high mobility prevent them from remaining on the surface. The molecules randomly diffuse on the surface and finally accumulate at the lower energy growth sites. Thus, the general indication of the VS growth process is the decrease of the diameter/width of the nanostructures toward their growth end. On the other hand, in the VLS process a thin layer of metal catalyst such as Au is deposited on the substrate, which at high temperature breaks up to form liquid nanodroplets. These metal droplets absorb the incoming source molecular vapor, and finally, upon supersaturation, solid naostructures start appearing with the metal nanoparticles at their tips. So, the characteristic of the VLS growth process is the existence of the metal nanoparticles at the tip of the nanostructures. In the present case, the SEM (Figures 2 and 3) and TEM studies (Figure 5a) reveal the presence of the Au nanoparticles at the front of the CdS nanoribbons, confirming the role of the VLS process. But the rectangular cross-section and the swordlike morphology of the CdS nanoribbons suggest that the conventional VLS process alone cannot be the growth mechanism. The TEM image shown in Figure 5b reveals the narrowing width and the rough side surfaces toward the growth front of the CdS nanoribbons. This image clearly indicates the role of the VS method in the growth

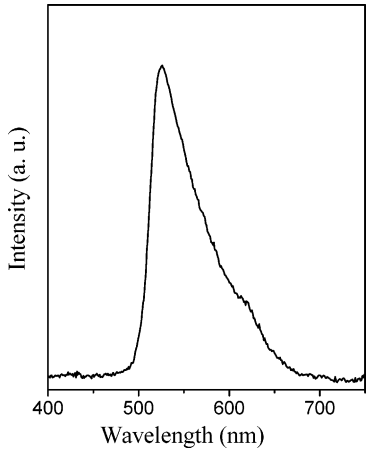

Figure 6. Photoluminescence spectrum of the CdS nanoribbons recorded at room temperature.

of these CdS nanoribbons. Thus, on the basis of these observations, we propose that both the VS and VLS processes are equally responsible for the growth of CdS nanoribbons, and the schematic representation of the growth model is given in Figure 5c. Since the growth of the CdS nanoribbons is initiated by the Au catalyst nanoparticles via the VLS process, controlling the sizes of the Au nanoparticles may be useful in controlling the thicknesses of the CdS nanoribbons. Also, the difference in the morphology of the CdS nanoribbons with different Ar flow rates might be due to the fact that, at higher Ar flow rate, the Au nanodroplets start moving on the substrate, resulting in the formation of assemblies of nanodroplets at different places and at the downstream edge. But, as the substrate was very close to the source, before the Au nanodroplets could merge to form a large droplet, the nucleation of the CdS nanoribbons started and finally stars like assemblies of CdS nanoribbons appeared. Increase in the growth temperature increased the mobility of the CdS molecules, resulting in the fast growth of CdS nanoribbons, and hence longer nanoribbons were observed at higher temperature. In addition, the position of the substrates that were very close to the CdS source (~3 mm) might have helped the rapid formation of the nanoribbons.

3.4. Photoluminescence Properties. The optical properties of the CdS nanoribbons were investigated by PL measurements at room temperature with a view to further assess their quality. Figure 6 shows the room-temperature PL spectrum recorded over the CdS nanoribbons with 400 nm excitation. Intense green emission centered on 525 nm (2.36 eV) was observed. The band at 525 nm was due to the near band edge emission. Similar near band edge emissions from CdS nanowires and nanoribbons were also reported by several other groups [20,26] Defect-related red emission originated from the trapped states was also reported in CdS nanowires.[27] In the present case, the absence of such defect-related emission from the nanoribbons demonstrates that these CdS nanoribbons have excellent optical property and could be used to fabricate photonic devices. Despite the absence of any prominent defect-related PL peaks, the existence of some low-intensity peaks just below the band edge could not be ruled out, as the radiative centers are always present surrounding the surfaces of the nanoribbons due to their high surface-to-volume ratio. The fluctuation in the surface charge density and local fields result in the inhomogeneous broadening of the excitonic peaks.[28] The influence of surface is revealed from the broad asymmetric emission toward the higher wavelength, and these emissions originated from the surface donor−acceptor pair (DAP) recombinations.[28]

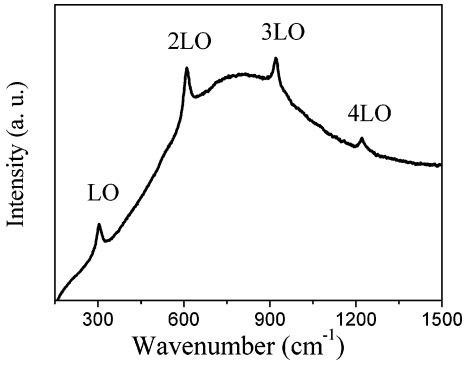

Figure 7. Raman spectrum of the CdS nanoribbons.

3.5. Raman Studies. Raman spectroscopy is a powerful tool for the investigation of doping concentration, lattice defect identification, and crystal orientation properties of the materials. Figure 7 shows the Raman spectrum recorded over a bunch of CdS nanoribbons with the characteristics Raman peaks analogous to the pure crystalline CdS.[29,30] The peaks at 305, 609, 915, and 1215 cm^{-1} correspond to the first-order (1-LO), second-order (2-LO), third-order (3-LO), and fourth-order (4-LO) longitudinal optical phonon bands of CdS, respectively. The high background of the Raman spectra could be attributed to the emission from the CdS nanoribbons.

4. Conclusions

In summary, rapid production of ultralong CdS nanoribbons with wurtzite structure have been achieved. It has been established that the flow rate of the Ar gas can also play an important role in determining the size and shape of the CdS nanoribbons. SEM and TEM studies indicated that the growth of the nanoribbons was governed by the combined effect of VS and Au-mediated VLS processes. Intense green emission from the nanoribbons at room temperature was centered at ~525 nm, which could be attributed to the near band edge emission. The Raman spectroscopic observations revealed the characteristics of well-crystallized pure CdS crystals. The smooth end and side surfaces along with uniform cross-sections of the nanoribbons make them a suitable candidate for the fabrication of nanolasers and other nanoscale devices.

References and Notes

(1) Iijima, S. *Nature* **1991**, *354*, 56.
(2) Rao, C. N. R.; Deepak, F. L.; Gundiah, G.; Govindaraj, A. *Prog. Solid State Chem.* **2003**, *31*, 5.
(3) Han, W. Q.; Fan, S. S.; Li, Q. Q.; Hu, Y. D. *Science* **1997**, *277*, 1287.
(4) Morales, A. M.; Lieber, C. M. *Science* **1998**, *279*, 208.
(5) Lieber, C. M. *Solid State Commun.* **1998**, *107*, 607.
(6) Heath, J. R.; Kuekes, P. J.; Snyder, G. S.; Williams, R. S. *Science* **1998**, *280*, 1716.
(7) Hu, J.; Ouyang, M.; Yang, P.; Lieber, C. M. *Nature* **1999**, *399*, 48.
(8) Wada, Y.; Yin, H.; Kitamura, T.; Yanagida, S. *Chem. Commun.* **1998**, *24*, 2683.
(9) Falcony, C.; Garcia, M.; Ortiz, A.; Alonso, J. C. *J. Appl. Phys.* **1992**, *72*, 1525.
(10) Pan, Z. W.; Dai, Z. R.; Wang, Z. L. *Science* **2001**, *291*, 1947.
(11) Li, Y. B.; Bando, Y.; Sato, T.; Kurashima, K. *Appl. Phys. Lett.* **2002**, *81*, 144.
(12) Arnold, M. S.; Avouris, P.; Pan, Z. W.; Wang, Z. L. *J. Phys. Chem B* **2003**, *107*, 659.
(13) Dai, Z. R.; Pan, Z. W.; Wang, Z. L. *J. Phys. Chem. B* **2002**, *106*, 902.
(14) Kong, X. Y.; Wang, Z. L *Solid State Commun*. **2003**, *128*, 1.
(15) Bae, S. Y.; Seo, H. W.; Park, J. *Appl. Phys. Lett.* **2002**, *81*, 126.
(16) Jiang, Y.; Meng, X. M.; Liu, J.; Xie, Z. Y.; Lee, C. S.; Lee, S. T. *Adv. Mater*. **2003**, *15*, 323.
(17) Kar, S.; Chaudhuri, S. *J. Phys. Chem B* **2005**, *109*, 3298.
(18) Dong, L.; Jiao, J.; Coulter, M.; Love, L. *Chem. Phys. Lett*. **2003**, *376*, 653.
(19) Duan, X.; Niu, C.; Sahi, V.; Chen, J.; Parce, J. W.; Empedocles, S.; Goldman, J. L. *Nature* **2003**, *425*, 274.
(20) Liu, Y. K.; Zapien, J. A.; Geng, C. Y.; Shan, Y. Y.; Lee, C. S.; Lee, S. T. *Appl. Phys. Lett.* **2004**, *85*, 3241.
(21) Zhang, J.; Jiang, F.; Zhang, L. *J. Phys. Chem. B* **2004**, *108*, 7002.
(22) Agata, M.; Kurase, H.; Hayashi, S.; Yamamoto, K. *Solid State Commun.* **1990**, *76*, 1061.
(23) Ullrich, B.; Bagnall, D. M.; Sakai, H.; Segawa, Y. *Solid State Commun.* **1999**, *109*, 757.
(24) Artemyev, M. V.; Sperling, V.; Woggon, U. *J. Appl. Phys.* **1997**, *81*, 6975.
(25) Duan, X. F.; Huang, Y.; Agarwal, R.; Lieber, C. M. *Nature* **2003**, *421*, 241.
(26) Mukherjee, P. K.; Chakravorty, D. *J. Appl. Phys.* **2004**, *95*, 3164.
(27) Wang, Y.; Meng, G.; Zhang, L.; Liang, C.; Zhang, J. *Chem. Mater*. **2002**, *14*, 1773.
(28) Ip, K. M.; Wang, C. R.; Li, Q.; Hark, S. K. *Appl. Phys. Lett.* **2004**, *84*, 795.
(29) Leite, R. C. C.; Porto, S. P. S. *Phys. Rev. Lett.* **1966**, *17*, 10.
(30) Suh, J. S.; Lee, J. S. *Chem. Phys. Lett.* **1997**, *281*, 384.